Bandgap Modulation in ZnO by Size, Pressure, and Temperature

J. W. Li,[†] L. W. Yang,*[,†,‡] Z. F. Zhou,[†] Paul K. Chu,[‡] X. H. Wang,[§] J. Zhou,[§] L. T. Li,[§] and Chang Q. Sun*[,∥]

Institute for Quantum Engineering and Micro-Nano Energy Technology and Faculty of Materials and Optoelectronic Physics, Xiangtan University, Hunan 411105, China, Department of Physics and Materials Science, City University of Hong Kong, Tat Chee Avenue, Kowloon, Hong Kong, China, State Key Lab of New Ceramics and Fine Processing, Department of Materials Science and Engineering, Tsinghua University, Beijing, 100084, China, and School of Electrical and Electronic Engineering, Nanyang Technological University, Singapore 639798, Singapore

Received: May 8, 2010; Revised Manuscript Received: June 26, 2010

The effect of crystal size, pressure, temperature, and their coupling on the bandgap (E_G) of ZnO crystals have been investigated based on the Hamiltonian perturbation, using the extended BOLS correlation theory. The functional dependence of the E_G on the identities (order, nature, length, energy) of the representative bond for a specimen and the response of the bonding identities to the applied stimuli have been established. Theoretical reproduction of the measurements confirms that the E_G expansion originates from the bond contraction/compression and bond strength gain due to (i) Goldschmidt−Pauling's rule of bond contraction induced by undercoordination, (ii) low-temperature enhanced stability, and (iii) mechanical energy storage. It is found that the multiple-field coupling effect dominates in the surface skin up to three atomic layers. The presented approach provides a guideline for harnessing the photoluminescence, photoabsorption, and exciton emission from ZnO and other semiconductors as well.

I. Introduction

As a wide bandgap semiconductor with high exciton binding energy (~60 meV), ZnO nanostructures have potential applications in high-efficiency short-wavelength optoelectronic nanodevices such as room temperature ultraviolet (UV) laser, UV detector, and photoluminescence (PL) sources.[1−5] Hence, deeper insight into the size-dependent optical properties of ZnO nanostructures under the externally applied stimuli of temperature and pressure is important from both fundamental and application points of view.

As a result of structural miniaturization, a blue shift can often be observed from the PL and photoabsorption (PA) of ZnO nanostructures. The bandgap (E_G), PL (E_{PL}), and PA (E_{PA}) energies of ZnO nanocrystals,[6−11] nanorods,[12,13] nanobelts,[14] and nanofilms[15] increase when the size diminishes or the shape is changed from one-dimension to three-dimensions for the same feature size. Moreover, the PL, PA, and E_G of ZnO nanostructures undergo blue shift with decreasing temperatures[16−19] or increasing external pressure.[20−23] A number of theoretical models have been developed to study the size-induced blue shift of PL, PA, and E_G in ZnO nanostructures including the quantum confinement,[11,24] color centers,[25] free-exciton collision,[26] surface states,[12,27] and Burstein−Moss effect,[13] as well as the classical thermodynamic approach.[28,29] These models explained reasonably well the PL blue shift but not for both the PL and the PA simultaneously. The thermally and mechanically induced E_G shift were usually fitted by using the following empirically quadratic functions:[19,20,30]

$$E_G(T) = E_G(0) - AT^2/(B + T)$$

$$E_G(P) = E_G(0) + CP + DP^2$$

where $E_G(0)$ is bandgap at 0 K and under the ambient pressure, and A, B, C, and D are adjustable parameters without clear physical indications. Although these equations can be used to numerically fit the measurements, the underlying physical mechanism remains yet ambiguous. Therefore, comprehensive understanding of the effect of size, pressure, and temperature and their coupling on the E_G shift is highly desired. Here we report an analytic solution connecting the E_G directly to the bonding identities (order, nature, length, energy) of a representative bond for a specimen and their response to the applied stimuli for a better understanding of the mechanism behind them. The multiple-fields coupling effect is formulated based on the bond order−length−strength (BOLS) correlation mechanism[31] and the local bond average (LBA) approach.[32] Theoretical reproduction of the measurements reveals that the multiple-field effect on the E_G originates from the Hamiltonian perturbation due to (i) the broken-bond-induced local strain and quantum entrapment of energy in the surface skin up to two atomic layers in depth, (ii) the thermally induced red shift arising from bond expansion and bond weakening due to lattice vibration, (iii) the pressure-induced blue shift resulting from bond strengthening due to mechanical work hardening, and (iv) the coupling effect happening only in the skin region of the specimen.

II. Principle

According to the nearly free electron approximation, the E_G between the conduction and the valence band depends uniquely on the first Fourier coefficient of the crystal potential, E_G =

* To whom correspondence should be addressed. E-mail: ylwxtu@xtu.edu.cn (L.W.Y.) and ECQSun@ntu.edu.sg (C.Q.S.).
[†] Xiangtan University.
[‡] City University of Hong Kong.
[§] Tsinghua University.
[∥] Nanyang Technological University.

10.1021/jp104204y
Published on Web 07/19/2010

$2|V_1| \propto \langle E_b \rangle$, which is proportional to the mean cohesive energy per bond $\langle E_b \rangle$, where $V_1 = \int V_{cry}(r) e^{ik\cdot r}\, dr$. With a given set of Bloch wave functions $|\varphi(k,r)\rangle$, under equilibrium conditions, the interatomic potential $V_{cry}(r)$ determines the intrinsic E_G, which has little to do with the density or energy of the excitons that dictate the quantum confinement effect. Therefore, any perturbation to the $V_{cry}(r=d) \propto E_b$ will modify the E_G intrinsically, if the $|\varphi(k,r)\rangle$ changes insignificantly with solid size or when subjected to external stimulus such as the change of the temperature and pressure. From the perspective of the LBA approach, the perturbation to the crystal potential or to the $\langle E_b \rangle$ of a nanosolid under the applied temperature and pressure can be divided into three contributions,[32]

$$\Delta_H = \sum_x \Delta_x \tag{1}$$

where $x = K$, T, and P denotes the perturbation introduced by size, temperature, and pressure, respectively.

Recently, we explored the size-induced E_G expansion of ZnO nanostructures based on the BOLS correlation and confirmed that the size trend was dominated by a limited number (≤ 3) of surface atoms while bonds in the core interior retained their bulk nature.[33] Taking the contributions of bonds between atoms in the outermost three atomic layers into consideration, the crystal potential and the associated E_G of a nanosolid containing N atoms undergo a perturbation, Δ_K,

$$\begin{aligned} V_{cry}(K) &= V_{cry}(\infty)(1 + \Delta_K) \\ \Delta_K &= \frac{V_{cry}(K) - V_{cry}(\infty)}{V_{cry}(\infty)} = \frac{E_G(K) - E_G(\infty)}{E_G(\infty)} = \\ &\quad \sum_{i\leq 3} \gamma_i \left(\frac{E_{i0}}{E_{b0}} - 1 \right) = \sum_{i\leq 3} \gamma_i (c_i^{-m} - 1) \\ \gamma_i &= \frac{V_i}{V} = \tau c_i K^{-1} \end{aligned} \tag{2}$$

where V_i is the volume of the ith layer, K is the dimensionless form of size or the number of atoms lined along the radius of a sphere or across the thickness of a thin film, γ_i is the surface-to-volume ratio of different dimensionality, τ is the dimensionality, and $\tau = 3$, 2, 1 for a nanodot, a nanorod, or a nanofilm, respectively, and i denotes the ith atomic layer, which may be counted up to three from the outermost atomic layer to the center of the solid. The m for ZnO has been optimized as 2.4.[33,34] E_{i0} and E_{b0} are the cohesive energy per bond of an atom in the ith atomic layer and the bulk without the external pressure at 0 K, respectively. According to the BOLS correlation, if one bond breaks, the remainder between the under-coordinated atoms will contract from the bulk value of d_0 to $d_i = c_i d_0$ and the cohesive energy per bond will increase from the bulk value of E_{b0} to $E_{i0} = c_i^{-m} E_{b0}$. c_i is the Goldschmidt−Pauling's coefficient of bond contraction and $c_i = d_i/d_0 = \{1 + \exp[(12 - z_i)/(8z_i)]\}^{-1}$, which replicates Goldschmidt−Paulings' convention of "atomic coordination size". The effective coordination number, z_i, of a specific atom in the ith atomic layer is curvature dependent, which satisfies the relation of $z_1 = 4(1 - 0.75/K)$, $z_2 = z_1 + 2$, and $z_3 = z_b = 12$, where z_b is the effective atomic coordination number in bulk.[31]

Under the applied temperature and pressure, the change in the bond energy $E(T,P)$ follows the relationship[32]

$$E(T,P) = E_{x0}\left\{1 - \frac{1}{E_{x0}}[\Delta_{xP} + \Delta_{xT}]\right\} \quad (x = i, b) \tag{3}$$

Physically, the distortion energy gain, Δ_p, should be equal to its mechanical work due to unit cell compression under the external pressure, which corresponds to the area of $V_0 \Delta S$ in the $V-P$ profile, which can be written as[32]

$$\Delta_p = -\int_{V_0}^{V} p(v)\, dv = -\int_1^{V/V_0} p(v)\, dx = [\int_0^P v\, dp - VP]/V_0 \tag{4}$$

The V and P are correlated with the Birch Mürnaghan isothermal equation of state[32]

$$P(v) = \frac{3B_0}{2}(\xi^{-7/3} - \xi^{-5/3})\left\{1 + \frac{3}{4}(B'_0 - 4)(\xi^{-2/3} - 1)\right\} \tag{5}$$

where P is the external pressure, B_0 is the static bulk modulus, and B'_0 is the first-order pressure derivative of the B_0; the $\xi = V/V_0$ is the ratio of volume of unit cell addressed after and before being compressed, and V_0 is the volume of unit cell at 0 K and 0 Pa. According to Debye approximation, the temperature-induced bond energy depression, (Δ_T), follows the relationship:

$$\begin{aligned} \Delta_T &= \int_0^T \eta_1(T)\, dt = \int_0^T \frac{C_V(T/\theta_D)}{z}\, dt \\ &= \int_0^T \int_0^{\theta_D/T} \frac{9R}{z}\left(\frac{T}{\theta_D}\right)\frac{x^4 \exp(x)}{(e^x - 1)^2}\, dx\, dt = \\ &\quad \frac{9RT}{z}\left(\frac{T}{\theta_D}\right)^3 \int_0^{\theta_D/T} \frac{x^3}{e^x - 1}\, dx \end{aligned} \tag{6}$$

where $\eta_1(T)$ is the specific heat per bond, which follows approximately the specific heat of the Debye approach and closes to a constant value of $3R$ (R is the ideal gas constant) at high temperature.[35] R, θ_D, C_V, and z are the idea gas constant, Debye temperature, specific heat, the nearest neighboring atom number of a given atom, respectively.

On the other hand, the conventional cohesive energy that is defined as the energy required to break the atoms of the solid into isolated atoms, (E_{coh}), of a nanosolid containing N atoms under the joint effect of multiple fields can be integrated based on the rule of energy superposition. The bond energy change due to the external stimuli perturbs the Hamiltonian, being the same as the size effect based on the core−shell configuration[32,36]

$$E_{coh}(K,P,T) = z_b E_b (N - \sum_{i\leq 3} N_i) + \sum_{i\leq 3} N_i z_i E_i$$

where

$$\begin{cases} E_i = E_{i0} + \sum_x \Delta E_{ix} \\ E_b = E_{b0} + \sum_x \Delta E_{bx} \end{cases} \quad (x = T, P)$$

Considering the multiple-fields coupling and the relation of $E_{coh}(\infty,0,0) = N z_b E_{b0}$, we have

$$E_{coh}(K,P,T) = z_b(E_{b0} + \Delta_{bP} + \Delta_{bT})(N - \sum_{i\le 3} N_i) + \sum_{i\le 3} N_i z_i (E_{i0} + \Delta_{iP} + \Delta_{iT})$$

and

$$\begin{aligned}\frac{E_{coh}(K,T,P)}{E_{coh}(\infty,0,0)} &= \left(1 + \frac{\Delta_{bT} + \Delta_{bP}}{E_{b0}}\right)(1 - \sum_{i\le 3}\gamma_i) + \sum_{i\le 3}\gamma_i z_{ib}\left(c_i^{-m} + \frac{\Delta_{iT} + \Delta_{iP}}{E_{b0}}\right)\\ &= \left(1 + \frac{\Delta_{bT} + \Delta_{bP}}{E_{b0}}\right) + \sum_{i\le 3}\gamma_i\left[(z_{ib}c_i^{-m} - 1) + z_{ib}\frac{\Delta_{iT} + \Delta_{ip}}{E_{b0}} - \frac{\Delta_{bT} + \Delta_{bP}}{E_{b0}}\right]\\ &= [1 + \sum_{i\le 3}\gamma_i(z_{ib}c_i^{-m} - 1)] + \frac{\Delta_{bT} + \Delta_{bP}}{E_{b0}}\left[1 + \sum_{i\le 3}\gamma_i\left(z_{ib}\frac{\Delta_{iT} + \Delta_{iP}}{\Delta_{bT} + \Delta_{bP}} - 1\right)\right]\\ &= [1 + \sum_{i\le 3}\gamma_i(z_{ib}c_i^{-m} - 1)] + \frac{\sum_x \Delta_{bx}}{E_{b0}}\left[1 + \sum_{i\le 3}\gamma_i\left(z_{ib}\frac{\sum_x \Delta_{ix}}{\sum_x \Delta_{bx}} - 1\right)\right]\\ &\quad (\chi = T, P, z_{ib} = z_i/z_b)\end{aligned} \tag{7}$$

The first part represents the effect of size and the second the joint effect of temperature and pressure on the atomic cohesive energy. It shows clearly that multifield-coupling effect occurs only in the surface skin (see the second part in the second term in eq 7). If the particle is insufficiently small we can take the approximation, $\Delta_{ix}/\Delta_{bx} \approx 1$, and $\gamma_i \ll 1$.[36] Hence, eq 7 can be simplified as

$$\frac{\Delta E_{coh}(K,P,T)}{E_{coh}(\infty,0,0)} = \sum_{i\le 3}\gamma_i(z_{ib}c_i^{-m} - 1) + \frac{\Delta_{bT} + \Delta_{bP}}{E_{b0}} \tag{8}$$

Therefore, the functional dependence of E_G on size, temperature, and pressure can be established as follows:

$$\frac{\Delta E_G(K,P,T)}{E_G(\infty,0,0)} = \frac{z_b}{\langle z_b\rangle}\left[\sum_{i\le 3}\gamma_i(z_{ib}c_i^{-m} - 1) + \frac{\Delta_{bT} + \Delta_{bP}}{E_{b0}} + 1\right] - 1 \tag{9}$$

where $\langle z_b\rangle$ is the average atomic CN and equals $\langle z_b\rangle = z_b[1 + \sum_{i\le 3}\gamma_i(z_{ib} - 1)]$.

III. Results and Discussion

The well-measured size, temperature, and pressure dependence of PL, PA, and E_G in ZnO nanostructures allows us to verify the presently developed analytical solutions. In the numerical calculations, we adopt the known $z = 4$, $c_1 = 0.8756$ and $c_2 = 0.9376$,[31] $\theta_D = 310$ K, bulk modulus $B = 160$ GPa, $B'_0 = 4.4$,[37] $V_0 \cong 48$ Å^3 for ZnO,[38] and the thermal expansion coefficient $\alpha(t)$[39] as input. In ZnO crystal with wurtzite-type structure, the $\alpha(t)$ is anisotropic. The principal values of $\alpha(t)$ in these hexagonal structures are those perpendicular and parallel to the c-axis, which are denoted as α_a ($\alpha_a = 6.05 \times 10^{-6} + (2.20 \times 10^{-9})t + (2.29 \times 10^{-14})t^2$) and α_c ($\alpha_c = 3.53 \times 10^{-6} + (2.38 \times 10^{-9})t + (9.24 \times 10^{-14})t^2$),[39] respectively. The effective $\alpha(t)$ is an average of $(2\alpha_a + \alpha_c)/3$.[40] On the other hand, for $T > \theta_D$, the specific heat (C_V) approaches a constant value and the thermally induced bond energy has an approximately linear dependence on temperature. Hence the relative E_G shift at 0 Pa under the high temperature approximation can be expressed as

$$\frac{E(T,0)}{E(0,0)} = \left(1 - \frac{\eta_1 T}{E_b(0)}\right) = 1 - B \times T \tag{10}$$

The slope B_{exp} of the experimental data can be easily determined by linearly fitting the E_G shift versus T curve at high-temperature range. Using the relation of $B_{exp} \cong B = \eta_1/E_b(0)$ with $\eta_1 \equiv 3R/z$, the cohesive energy per bond $E_b(0)$ can be estimated. The optimized average $E_b(0)$ is ~0.75 eV for ZnO and then it is used as an initial input to refine the fitting to the experimental data in the entire temperature range by including the contribution of the nonlinear lattice thermal expansion.

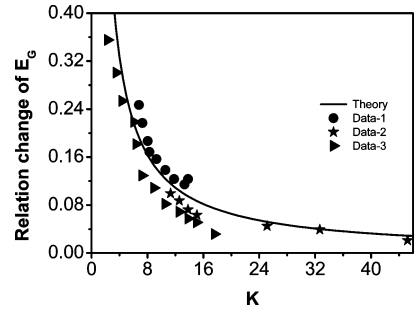

Figure 1. Theoretical (solid) reproduction of the measured size dependence of E_G for ZnO nanostructures at room temperature and under atmospheric pressure. The experimental data are sourced from refs 7 and 9−11.

Figure 1 shows the theoretical match of the measured size dependence of the relative change of E_G in ZnO nanostructures at room temperature and atmospheric pressure. For simplification, the pressure effect on the E_G shift is neglected and the bulk E_G value (3.26 eV) at room temperature is used. Consistency between prediction and measurement indicates that the impact of broken-bond-induced local strain and quantum trapping at the surface of skin depth dictates the E_G expansion.

Figure 2 shows the theoretical reproduction of the measured temperature-dependent E_G of ZnO nanostructures with different size and shape at atmospheric pressure in the entire temperature range. Similarly, the E_G value of ZnO nanostructures with different sizes are adjusted according to size change. One can find that for all nanostructures with different sizes, at $T \ge \theta_D/3$, the changes of E_G always turn from nonlinear to linear when the temperature is increased. The small change at very low temperatures arises from the small $\int_0^T \eta(t)\,dt$ values as the specific heat $\eta(t)$ is proportional to T^3 at very low temperature. The results imply that the Debye temperature (θ_D) determines the width of the shoulder and the $1/E_b(0)$ determines the slopes at

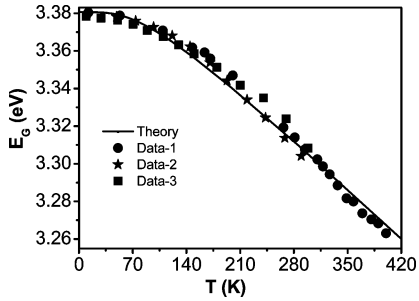

Figure 2. Theoretical (solid) reproduction of the measured temperature dependence of E_G for ZnO at atmospheric pressure. The experimental data are sourced from refs 16−18.

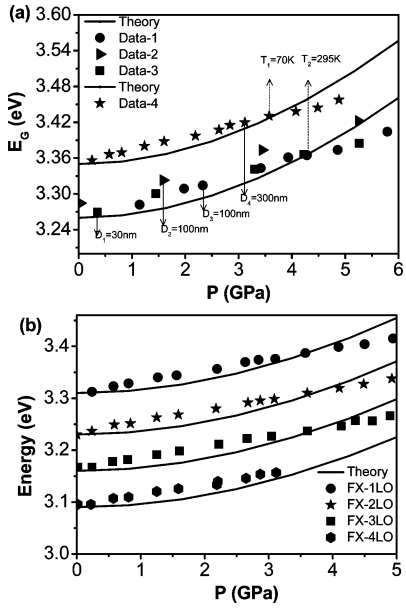

Figure 3. (a) Theoretical (solid) reproduction of the measured pressure dependence of E_G for ZnO at a variety of sizes and temperatures. The experimental data are sourced from refs 20−23; and (b) the measured pressure dependence of $E_{FX\text{-}n\mathrm{LO}}$ at 70 K. The experimental data are sourced from the ref 23.

high temperature in the curve showing the temperature-dependent E_G change. These results are very interesting since the trend of the temperature-dependent E_G shift is similar to that of the temperature-dependent Raman shift in ZnO.[35]

Figure 3a shows the consistency between BOLS predictions and the experimental results of pressure-dependent E_G at different temperatures and crystal sizes. Generally, the energy increases nonlinearly with pressure according to the Birch Mürnaghan-isothermal equation. This can be ascribed to the fact that the V/V_0 of the unit cell becomes smaller as the specimen is compressed. According to the results for different sizes and temperatures, the temperature effect should be included but the size effect is not apparent when the solid size is greater than 30 nm at which the surface-to-volume ratio is negligibly small. At the same temperature, good agreement between theory and measurement evidence that the pressure-induced E_G expansion in ZnO nanostructures mainly arises from the pressure-induced bond strengthening. Furthermore, it also implies that the multifield-coupling effect indeed occurs only in the surface skin, but this effect can be omitted for larger particle sizes. The relationship between E_G and the energy of the free exciton (E_{FX}) and its nth longitudinal optic (LO) phonon replicas can be expressed as $E_{FX\text{-}n\mathrm{LO}} = E_G + {}^3/_2 k_B T - n\hbar\omega_{LO}$, where k_B is the Boltzmann constant, $\hbar\omega_{LO}$ represents the LO phonon energy, and $\hbar\omega_{LO} = 72$ meV.[23] The application of pressure increases the binding energy of a shallow exciton arising from an increase of electron effective mass and a decrease in dielectric constant as the E_G increases. Besides, the energy of longitudinal optic (LO) phonon will also increase with the external pressure.[35] However, the pressure-induced increase in exciton binding and LO phonon of ZnO has been estimated to much less than that of the ZnO bandgap.[21,35] Therefore the effect of pressure on exciton emission originates likely from the E_G expansion of ZnO. According to the aforementioned discussion, we reproduce the experimental results of the pressure-dependent energy of free exciton (E_{FX}) and its nth LO phonon replicas measured at 70 K in ZnO nanostructures and the results are displayed in Figure 3b.

IV. Conclusion

We present an analytical expression connecting the macroscopically measurable E_G directly to the bonding identities of the specimen and their response to the intrinsic coordination-imperfection and the applied stimulus for deeper insight into the atomistic origin of the size-, temperature-, and pressure-induced E_G change in ZnO nanostructures through the BOLS correlation and the LBA approach. Theoretical reproduction of the measurements reveals that size-induced E_G expansion arises from the broken-bond-induced local strain and skin-depth quantum trapping, thermal induced E_G compression arises from bond weakening, and the pressure-induced E_G expansion results from bond strengthening in a solid specimen. Reducing particle size, lowering temperature, and increasing pressure can be taken as measures to expand the bandgap. The approach presented here provides a useful yet simple way to investigate the optical properties such as PL, PA, and exciton emission under the stimuli change of atomic coordination and thermal and mechanical activation in ZnO and other semiconducting nanostructures.

Acknowledgment. The project was supported by Grants from National Natural Science Foundation of China (Nos. 10802071 and 10772157), Hunan Province, China, and City University of Hong Kong Strategic Research Grant (SRG) No. 7008009.

References and Notes

(1) Huang, M. H.; Mao, S.; Feick, H.; Yan, H.; Wu, Y.; Kind, H.; Weber, E.; Russo, R.; Yang, P. *Science* **2001**, *292* (5523), 1897–1899.
(2) Xia, Y.; Yang, P.; Sun, Y.; Wu, Y.; Mayers, B.; Gates, B.; Yin, Y.; Kim, F.; Yan, H. *Adv. Mater.* **2003**, *15* (5), 353–389.
(3) Sun, X. W.; Wang, J. X. *Nano Lett.* **2008**, *8* (7), 1884–1889.
(4) Wu, X.; Siu, G.; Fu, C.; Ong, H. *Appl. Phys. Lett.* **2001**, *78*, 2285.
(5) Wang, Z.; Song, J. *Science* **2006**, *312* (5771), 242.
(6) Li, J.; Wang, L. *Phys. Rev. B* **2005**, *72* (12), 125325.
(7) Irimpan, L.; Nampoori, V. P. N.; Radhakrishnan, P.; Deepthy, A.; Krishnan, B. *J. Appl. Phys.* **2007**, *102* (6), 063524–6.
(8) Meulenkamp, E. A. *J. Phys. Chem. B* **1998**, *102* (29), 5566–5572.
(9) Ranjani Viswanatha, S. S.; Satpati, B.; Satyam, P. V.; Dev, B. N.; Sarma, D. D. *J. Mater. Chem.* **2004**, *14* (4), 661–668.
(10) Wood, A.; Giersig, M.; Hilgendorff, M.; Vilas-Campos, A.; Liz-Marz, L. M.; Mulvaney, P. *Aust. J. Chem.* **2003**, *56* (10), 1051–1057.
(11) Lin, K.-F.; Cheng, H.-M.; Hsu, H.-C.; Lin, L.-J.; Hsieh, W.-F. *Chem. Phys. Lett.* **2005**, *409* (4−6), 208–211.
(12) Chen, C.-W.; Chen, K.-H.; Shen, C.-H.; Ganguly, A.; Chen, L.-C.; Wu, J.-J.; Wen, H.-I.; Pong, W.-F. *Appl. Phys. Lett.* **2006**, *88* (24), 241905–3.
(13) Yang, Y.; Chen, X.; Feng, Y.; Yang, G. *Nano Lett.* **2007**, *7* (12), 3879–3883.
(14) Wang, X.; Ding, Y.; Summers, C.; Wang, Z. *J. Phys. Chem. B* **2004**, *108* (26), 8773–8777.
(15) Nie, J.; Yang, J.; Piao, Y.; Li, H.; Sun, Y.; Xue, Q.; Xiong, C.; Dou, R.; Tu, Q. *Appl. Phys. Lett.* **2008**, *93*, 173104.
(16) Alawadhi, H.; Tsoi, S.; Lu, X.; Ramdas, A. K.; Grimsditch, M.; Cardona, M.; Lauck, R. *Phys. Rev. B* **2007**, *75* (20), 205207.

(17) Ursaki, V. V.; Tiginyanu, I. M.; Zalamai, V. V.; Rusu, E. V.; Emelchenko, G. A.; Masalov, V. M.; Samarov, E. N. *Phys. Rev. B* **2004**, *70* (15), 155204.

(18) Eom, S. H.; Yu, Y. M.; Choi, Y. D.; Kim, C. S. *J. Cryst. Growth* **2005**, *284* (1−2), 166–171.

(19) Cao, B.; Cai, W.; Zeng, H. *Appl. Phys. Lett.* **2006**, *88* (16), 161101–3.

(20) Shan, W.; Walukiewicz, W.; Ager, J. W.; Iii; Yu, K. M.; Zhang, Y.; Mao, S. S.; Kling, R.; Kirchner, C.; Waag, A. *Appl. Phys. Lett.* **2005**, *86* (15), 153117–3.

(21) Chen, S. J.; Liu, Y. C.; Shao, C. L.; Xu, C. S.; Liu, Y. X.; Liu, C. Y.; Zhang, B. P.; Wang, L.; Liu, B. B.; Zou, G. T. *Appl. Phys. Lett.* **2006**, *88* (13), 133127–3.

(22) Huso, J.; Morrison, J. L.; Hoeck, H.; Chen, X.-B.; Bergman, L.; Jokela, S. J.; McCluskey, M. D.; Zheleva, T. *Appl. Phys. Lett.* **2006**, *89* (17), 171909–3.

(23) Hai Su, F.; Jie Wang, W.; Ding, K.; Hua Li, G.; Liu, Y.; Joly, A. G.; Chen, W. *J. Phys. Chem. Solids* **2006**, *67* (11), 2376–2381.

(24) Cheng, H.; Lin, K.; Hsu, H.; Hsieh, W. *Appl. Phys. Lett.* **2006**, *88*, 261909.

(25) Qin, G.; Song, H.; Zhang, B.; Lin, J.; Duan, J.; Yao, G. *Phys. Rev. B* **1996**, *54* (4), 2548–2555.

(26) Glinka, Y. D.; Lin, S.-H.; Hwang, L.-P.; Chen, Y.-T.; Tolk, N. H. *Phys. Rev. B* **2001**, *64* (8), 085421.

(27) Wang, X.; Qu, L.; Zhang, J.; Peng, X.; Xiao, M. *Nano Lett.* **2003**, *3* (8), 1103–1106.

(28) Guisbiers, G.; Van Overschelde, O.; Wautelet, M. *Appl. Phys. Lett.* **2008**, *92*, 103121.

(29) Guisbiers, G.; Pereira, S. *Nanotechnology* **2007**, *18*, 435710.

(30) Chen, S. J.; Liu, Y. C.; Shao, C. L.; Xu, C. S.; Liu, Y. X.; Wang, L.; Liu, B. B.; Zou, G. T. *J. Appl. Phys.* **2005**, *98* (10), 106106–3.

(31) Sun, C. Q. *Prog. Solid State Chem.* **2007**, *35* (1), 1–159.

(32) Sun, C. Q. *Prog. Mater. Sci.* **2009**, *54* (2), 179–307.

(33) Li, J.; Liu, X.; Yang, L.; Zhou, Z.; Xie, G.; Pan, Y.; Wang, X.; Zhou, J.; Li, L.; Pan, L. *Appl. Phys. Lett.* **2009**, *95*, 031906.

(34) Liu, X.; Li, J.; Zhou, Z.; Yang, L.; Ma, Z.; Xie, G.; Pan, Y.; Sun, C. *Appl. Phys. Lett.* **2009**, *94*, 131902.

(35) Li, J.; Yang, L.; Zhou, Z.; Liu, X.; Xie, G.; Pan, Y.; Sun, C. *J. Phys. Chem. B* **2010**, *114* (4), 1648–1651.

(36) Ouyang, G.; Sun, C.; Zhu, W. *J. Phys. Chem. C* **2009**, *113* (22), 9516–9519.

(37) Karzel, H.; Potzel, W.; Köfferlein, M.; Schiessl, W.; Steiner, M.; Hiller, U.; Kalvius, G. M.; Mitchell, D. W.; Das, T. P.; Blaha, P.; Schwarz, K.; Pasternak, M. P. *Phys. Rev. B* **1996**, *53* (17), 11425.

(38) Sowa, H.; Ahsbahs, H. *J. Appl. Crystallogr.* **2006**, *39* (2), 169–175.

(39) Khan, A. *Acta Crystallogr., Sect. A* **1968**, *24* (3), 403.

(40) Slack, G. A.; Bartram, S. F. *J. Appl. Phys.* **1975**, *46* (1), 89–98.

JP104204Y